Thermal decay of a metastable state: Influence of rescattering on the quasistationary dynamical rate

M. V. Chushnyakova[1,2,*] and I. I. Gontchar[1,3]
[1]*Physics Department, Omsk State Technical University, 644050 Omsk, Russia*
[2]*Physics Department, Akdeniz University, 07058 Antalya, Turkey*
[3]*Physics and Chemistry Department, Omsk State Transport University, 644046 Omsk, Russia*

(Received 8 August 2017; revised manuscript received 20 January 2018; published 12 March 2018)

We study the effect of backscattering of the Brownian particles as they escape out of a metastable state overcoming the potential barrier. For this aim, we model this process numerically using the Langevin equations. This modeling is performed for the wide range of the friction constant covering both the energy and spatial diffusion regimes. It is shown how the influence of the descent stage on the quasistationary decay rate gradually disappears as the friction constant decreases. It is found that, in the energy diffusion regime, the rescattering absents and the descent stage does not influence the decay rate. As the value of friction increases, the descent alters the value of the rate by more than 50% for different values of thermal energy and different shapes of the potential. To study the influence of the backscattering on the decay rate, four potentials have been considered which coincide near the potential well and the barrier but differ beyond the barrier. It is shown that the potential for which the well and the barrier are described by two smoothly joined parabolas ("the parabolic potential") plays a role of a dividing range for the mutual layout of the quasistationary dynamical rate and the widely used in the literature Kramers rate. Namely, for the potentials with steeper tails, the Kramers rate $R_{\rm KM}$ underestimates the true quasistationary dynamical rate R_D, whereas for the less steep tails the opposite holds (inversion of $R_D/R_{\rm KM}$). It is demonstrated that the mutual layout of the values of R_D for different potentials is explained by the rescattering of the particles from the potential tail.

DOI: 10.1103/PhysRevE.97.032107

I. INTRODUCTION

Escape of a Brownian particle from a potential well due to thermal fluctuations is relevant for many branches of natural sciences [1–15]. In his seminal paper [1] Kramers proposed several formulas for the rate of this decay. Here, we write down those in dimensionless form. One of these formulas is valid for the case of weak friction (energy diffusion regime). Including the modification proposed in Ref. [16] it reads:

$$R_{\rm KL} = 2\pi\gamma\,\frac{\delta-1}{\delta+1}R_{\rm TS}. \tag{1}$$

The last multiplier in Eq. (1) is called transition state rate and is equal to

$$R_{\rm TS} = \frac{1}{2\pi}\exp(-\varepsilon), \tag{2}$$

where

$$\varepsilon = \frac{\tilde{U}_b}{\theta}; \tag{3}$$

$\tilde{U}_b$ is the barrier height (in energy units); θ is the thermal energy. For example, in nuclear physics θ is equal to the temperature T measured in MeV, in chemical or molecular applications $\theta = k_B T$ (k_B is the Boltzmann constant).

The dimensionless parameter γ in Eq. (1) reads

$$\gamma = \frac{I_b\beta\varepsilon}{U_b}. \tag{4}$$

The dimensionless action I_b is evaluated from the left turning point q_l up to the location of the top of the barrier q_b (see Fig. 1):

$$I_b = 2\int_{q_l}^{q_b}\sqrt{2[U_b - U(q)]}dq, \tag{5}$$

where β is the dimensionless damping coefficient

$$\beta = \frac{\eta}{m\omega_c}. \tag{6}$$

The friction coefficient η should be taken in proper units, m denotes mass of the Brownian particle (the inertia parameter) in corresponding units; ω_c is the frequency of oscillations near the parabolic bottom of the potential well in units of inverse time. Following the previous description, the rates $R_{\rm KL}$ and $R_{\rm TS}$ are measured in units of ω_c. The dimensionless potential reads

$$U(q) = \frac{\tilde{U}(q)}{m\omega_c^2}, \tag{7}$$

where $\tilde{U}(q)$ is the potential energy of the Brownian particle in energy units.

The last unexplained ingredient of Eq. (1), δ, reads

$$\delta = \left(1 + \frac{2\alpha}{\pi\gamma}\right)^{1/2}. \tag{8}$$

*maria.chushnyakova@gmail.com

The coefficient α is a dimensionless adjustable parameter of the order of unity.

Equation (1) is valid if $\gamma \ll 1$. Since $\gamma = 1$ separates the energy diffusion regime from the opposite one ($\gamma > 1$), which is called "spatial diffusion regime" [11], let us call γ a separation parameter henceforth. For the latter regime one finds a different formula for the approximate quasistationary rate in Ref. [1]:

$$R_{\mathrm{KM}} = \left[\left(\frac{\omega_b^2}{\omega_c^2} + \frac{\beta^2}{4}\right)^{1/2} - \frac{\beta}{2}\right]\frac{\omega_c}{\omega_b} R_{\mathrm{TS}}. \tag{9}$$

Here ω_b is the frequencylike quantity calculated at the top of the barrier. We will refer to R_{KM} defined by Eq. (9) as to the Zero-order Kramers rate Formula (ZKF).[1]

The conditions of applicability of Eqs. (1) and (9) can be summarized as follows:

(i) the potential barrier is high enough comparing to the thermal energy θ;

(ii) the potential is represented well by the portions of parabolas near the quasistationary and barrier points.

Sometimes there are additional requirements for the rate (9) in the literature:

(iii) the absorptive border is far enough from the barrier;

(iv) the quasistationary point is far enough from the barrier.

The accuracy of ZKF has got some attention recently [17–22]. It was studied by comparison with the long time limit of the escape rate obtained using either the stochastic differential equations (the Langevin equations) [17,19,20,22] or the corresponding partial differential equation (the Smoluchowski equation) [18,21]. This limit is referred to as the Quasistationary Dynamical Rate (QDR) henceforth and denoted as R_D. Yet the accuracy of the approximate rate for the energy diffusion regime [see Eq. (1)], by our knowledge, was not studied carefully.

There are only the characteristics of the bottom of the well and of the barrier in both Eqs. (1) and (9); nothing tells us what happens to the particle which has overcome the barrier. In fact, after reaching the barrier, the particle can return to the quasistationary state due to fluctuations or move further to the absorptive point q_a due to the driving force. The absorptive point in nuclear fission corresponds to the scission point at which a nucleus separates quickly into two fragments. In general, the absorptive point is the last point from the top of the barrier where the Brownian particle can still be scattered back to the potential well. This rescattering can alter the value of the rate. Thus, the amount of agreement of the approximate Eqs. (1) and (9) with the exact quasistationary rate obtained in numerical modeling can depend upon the location of the absorbing border.

This dependence was considered in Refs. [18,23,24]. In these papers it was shown that ZKF agrees with the quasistationary dynamical rate only when the absorption point is far enough from the barrier point. In Refs. [18,22,23] it was shown that for the parabolic potential ZKF and QDR agree within typically 2% for different values of the thermal energy, barrier height and curvature. We consider this agreement to be a proof that all the rescatterings beyond the saddle are accounted for in the Kramers formula (9), although implicitly. Indeed, the Kramers flux over the barrier is the sum of positive (forward) and negative (backward) fluxes. This was shown analytically (see Eqs. (5) and (6) of Ref. [25]) and is seen in our dynamical modeling. The absorption point diminishes the backward flux thus making the net flux larger. The only case when the influence of this point disappears corresponds to the best agreement of the numerical rate with the Kramers one.

In the present work, we aim to study the impact of rescattering on the results of numerical modeling in the wide range of friction constant covering both the energy and spatial diffusion regimes. In particular, it is interesting to see what the influence of the potential shape beyond the barrier (i.e., between the barrier and the absorption point) on the agreement between the approximate analytical rate and R_D is. The paper is organized as follows. The model is described in Sec. II. Section III is devoted to the presentation of the results. In Sec. IV we summarize our conclusions.

II. THE MODEL

Our work stems from the nuclear fission problem which was mentioned in the original Kramers paper [1] as one of the examples of thermal decay of a metastable state. This problem involves several degrees of freedom (DOF) [8,15,20,26,27] and in Ref. [22] we studied the effects of multidimensionality on the accuracy of the Kramers-type approximate formula. However, later we realized that the rescattering problem is in fact related to the only DOF corresponding to the decay of the metastable state. Therefore, in the present work, the motion of the Brownian particle is characterized by a single collective coordinate q. In the case of nuclear fission, q is responsible for the elongation of the fissioning nucleus.

For the one-dimensional case, the Langevin equations in the differential form read

$$\begin{aligned} dq &= \tilde{p} m^{-1} d\tilde{t}, \\ d\tilde{p} &= -\left(\frac{\eta}{m}\tilde{p} + \frac{d\tilde{U}}{dq}\right) d\tilde{t} + \sqrt{2\eta\theta}\, d\tilde{W}. \end{aligned} \tag{10}$$

Here the coordinate q is dimensionless; all other quantities have physical dimensions. The increment $d\tilde{W}$ of the Wiener process $\tilde{W}$ possesses the normal distribution with the variance $d\tilde{t}$.This is the same time interval during which the momentum changes by $d\tilde{p}$ and the coordinate changes by dq.

The Langevin Eqs. (10) correspond to the following Fokker-Planck equation for the probability density $P(q,\tilde{p},\tilde{t})$:

$$\frac{\partial P}{\partial \tilde{t}} = -\frac{\partial}{\partial q}\left\{\frac{\tilde{p}}{m} P\right\} + \frac{\partial}{\partial \tilde{p}}\left\{\left(\frac{\eta}{m}\tilde{p} + \frac{d\tilde{U}}{dq} - \eta\theta\frac{\partial}{\partial \tilde{p}}\right) P\right\}. \tag{11}$$

Since the diffusion coefficient is in our case momentum independent, the Ito and Stratonovich interpretations of the Langevin Eqs. (10) coincide [28].

[1]Note that a simplified formula for the decay rate can be obtained from Eq. (9) provided $\beta^2/4 \gg 1$. For the latter case, the term "overdamped regime" ("overperiodically damped") is used often (see, e.g., Refs. [1,5,11,17]). Thus, the spatial diffusion regime is wider than the overdamped regime.

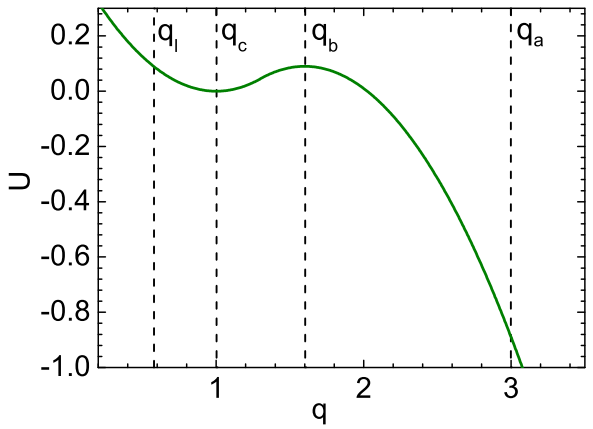

FIG. 1. The potential energy $U_P(q)$ with the metastable state (q_c). q_b indicates the position of the barrier; q_a reflects the possible location of the absorption point; q_l shows the left turning point [according to Eq. (5) $U_P(q_l) = U_b$].

The values of all quantities entering Eqs. (10) and (11) significantly depend upon the particular physical problem which the Langevin equations are used for. Nevertheless, the main features of thermal decay of a metastable state are common. Therefore, it is useful to convert these equations into dimensionless form to exclude particularities and to emphasize commonness:

$$dq = pdt,$$
$$dp = -\left(\beta p + \frac{dU}{dq}\right)dt + \sqrt{2\beta\frac{U_b}{\varepsilon}}dW. \tag{12}$$

The quantities $\tilde{t},\tilde{p},d\tilde{W}$ are related with the dimensionless ones t,p,dW as follows:

$$t = \tilde{t}\omega_c, \tag{13}$$

$$p = \frac{\tilde{p}}{m\omega_c}, \tag{14}$$

$$dW = d\tilde{W}\omega_c^{1/2}. \tag{15}$$

Relations of the quantities $\eta,\tilde{U},\theta$ with β,U,ε are given by Eqs. (6), (7), and (3), respectively. The discretized version of Eqs. (12) used for the computer modeling is presented in the Appendix.

Let us first concentrate on the influence of the damping coefficient on the backscattering. For this aim, we use the potential $U_P(q)$ represented by two parabolas of the same stiffness $C = U_b/(q_b - q_c)^2$ smoothly jointed at $q_m = (q_b + q_c)/2$ ("parabolic potential"):

$$U_P(q) = \begin{cases} C(q-q_c)^2/2 & \text{at } q < q_m; \\ U_b - C(q-q_b)^2/2 & \text{at } q > q_m. \end{cases} \tag{16}$$

For the quasistationary and barrier coordinates, we use $q_c = 1.00$, $q_b = 1.60$. The potential energy $U_P(q)$, as well as q_c and q_b, are shown in Fig. 1.

Initially (at $t = 0$) the Brownian particle is located at the minimum of the potential well ($q = q_c$, $p = 0$).

The modeling results in a sequence of $N_{\rm tot}$ trajectories, all of them are terminated not later than at $t = t_D$. Some of these

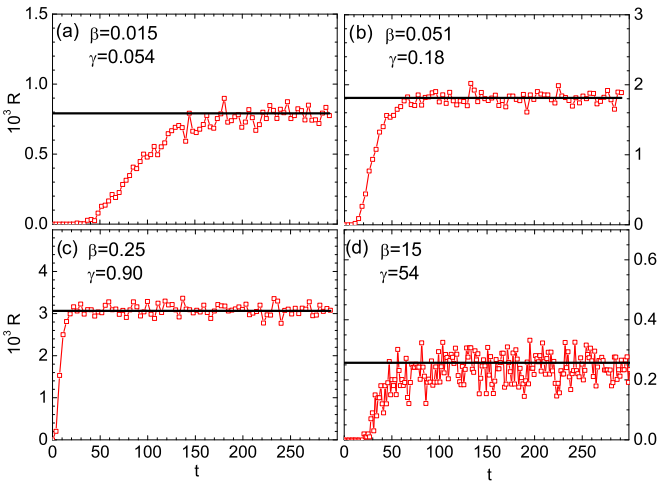

FIG. 2. The time dependence of the dynamical rates for four values of the dimensionless damping coefficient β (and separation parameter γ). The horizontal lines indicate the quasistationary dynamical rates. These calculations are performed for $\varepsilon = 3.74$.

trajectories reach the absorptive border q_a (see Fig. 1) before t_D. The dimensionless decay rate is then calculated as follows:

$$R_a(t) = \frac{1}{N_{\rm tot} - N_{\rm at}}\frac{\Delta N_{\rm at}}{\Delta t}. \tag{17}$$

Here $N_{\rm at}$ is the number of trajectories which have reached q_a by the time moment t; $\Delta N_{\rm at}$ is the number of trajectories which have reached the absorptive border during the time interval Δt (note, that we measure time in units of ω_c^{-1}). Several examples of $R_a(t)$-dependence are shown in Fig. 2 (see also Fig. 8 below). One sees that after some transient time, the dynamical rate reaches a quasistationary value R_D. In order to find R_D we take several bins backwards from the end of R_a-array (i.e., from the time moment t_D) and calculate the mean value of R_a over these bins (see details in Ref. [22]).

III. RESULTS

A. The influence of the damping coefficient

We start from the dynamical modeling with different locations of the absorption point and calculate the $R_D(q_a)$-dependence for several values of γ. The parabolic potential [Eq. (16)] is used in these calculations. Corresponding results are presented in Fig. 3 as the ratio R_{Db}/R_{Da}. Here R_{Db} is the dynamical quasistationary rate calculated when the absorption point is positioned exactly at the barrier ($q_a = q_b$), whereas R_{Da} is calculated at the varied absorption point q_a. We see that for $\gamma > 1$, $R_{Db} > R_{Da}$, whereas for the energy diffusion regime ($\gamma = 0.10$) $R_{Db} = R_{Da}$. We expected the latter result because in the energy diffusion regime the decay process is described by the diffusion equation (see, e.g., Eq. (14) of Ref. [1]) which does not include the coordinate at all.

For the spatial diffusion regime, the value of R_{Da} gradually increases with q_a reaching a saturated value of R_{Das}. This results in saturation of the R_{Db}/R_{Da} ratio. The saturated value of this ratio,

$$r_s = \frac{R_{Db}}{R_{Das}}, \tag{18}$$

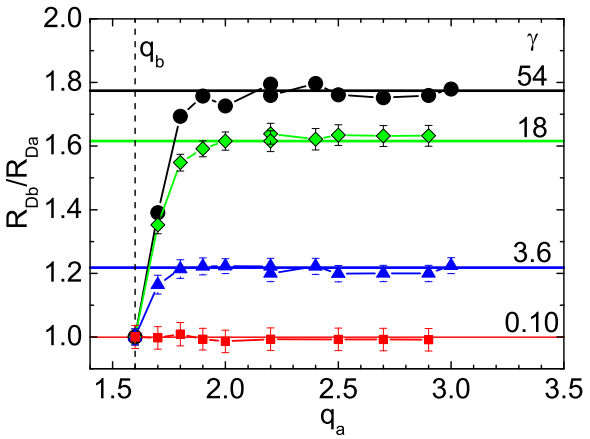

FIG. 3. The ratio of the dynamical quasistationary rates found at the fixed barrier point q_b and at the varied absorption point q_a, R_{Db}/R_{Da}, versus q_a. The horizontal lines correspond to $r_s = R_{Db}/R_{Das}$ (see text).

is not equal to 2 as it was thought earlier [17,21] but depends regularly upon the separation parameter (or equivalently upon the friction strength).

It looks like the separation parameter γ defined by Eq. (4) is not really good for characterizing the friction strength in the whole range of our calculations. Indeed, it nicely separates the energy diffusion regime from the spatial diffusion regime. Moreover, γ enters the analytical rate R_{KL}. However, as we enter the spatial diffusion regime, the separation parameter becomes irrelevant or even misleading. One can notice that γ includes the thermal energy in the denominator [see Eq. (4)], whereas R_{KM} depends upon θ only exponentially. This is why we prefer using the dimensionless damping coefficient β instead of γ below.

The dependence of the rates and r_s upon β is shown in Fig. 4. We see that our calculations cover more than three orders of magnitude in damping coefficient and two orders of magnitude in the rate. Of cause, for extremely small and large values of the damping coefficient, the calculations become increasingly computer time consuming. It is tempting to employ the reduced Langevin equations for the overdamping regime ($\beta \gg 1$) and the energy diffusion equation for $\beta \ll 1$. However, this would contradict the purpose of our study.

In Fig. 4(a) the solid circles indicate the values of R_{Das} whereas the triangles up stand for R_{Db}. These two rates are different only for $\beta > 0.1$. When we put the absorption point at the barrier (the way R_{Db} is calculated) we obtain the decay rate significantly larger than with the absorption point beyond the barrier (R_{Das}). The reason for that is the backscattering of the particles in the latter case. For comparison, we show in Fig. 4(a) the approximate rates R_{KM} and R_{KL} (lines) each in its domain of applicability. These analytical rates agree nicely with R_{Das} in the whole range of damping coefficient.

In Fig. 4(b) the value of r_s gradually grows with β from unity for the energy diffusion regime up to approximately 2 for the overdamping regime. This is what we wanted to clarify.

Results of Fig. 4 have been obtained for $\varepsilon = 3.00$. The natural question is to what extent the gradual increase of r_s is influenced by the value of ε. Thus, we performed extra

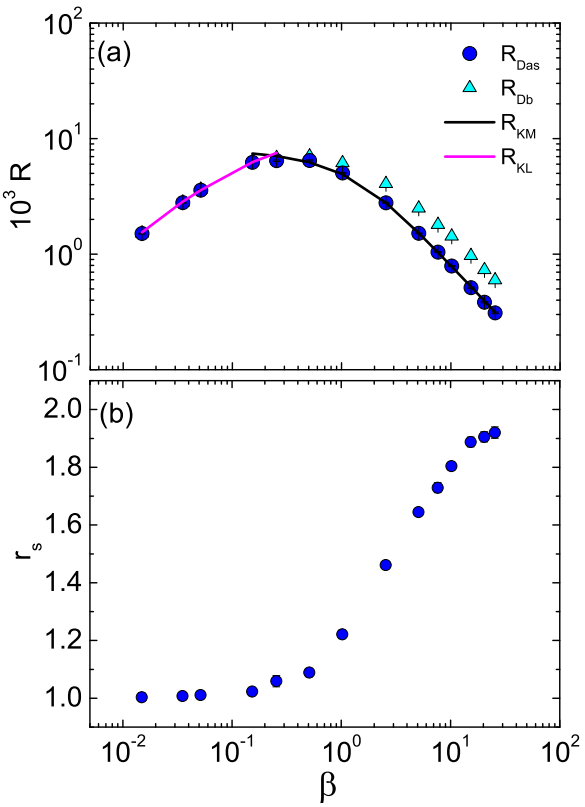

FIG. 4. The decay rates (a) and the saturated value of the rate ratio r_s (b) versus the dimensionless damping coefficient β. In panel (a) the solid circles, triangles up, and lines correspond to R_{Das}, R_{Db}, R_{KM} (the right part), and R_{KL} (the left part), respectively. $\varepsilon = 3.00$.

calculations for $\varepsilon = 3.74$. The calculated values of the rates and r_s obtained for these two values of ε are compared in Fig. 5. We see that the rates differ in these two cases by a factor of 2 [Fig. 5(a)], whereas the ratios r_s are nearly indistinguishable [Fig. 5(b)].

Finally, we would like to discuss what is the impact of the potential shape on the $r_s(\beta)$-dependence. For this aim, we construct the third-order polynomial (cubic) potential, which coincides with the parabolic one at q_c and q_b. The cubic potential is somewhat stiffer both at q_c and q_b. The rates calculated at $\varepsilon = 3.00$ for these two potentials are displayed in Fig. 6. In Fig. 6(a) we see that the rates R_{Das} for the cubic and parabolic potentials are very close. This is expected because the rates are mostly influenced by the controlling parameter ε (i.e., by the temperature and barrier height). However, the values of the ratios r_s(cubic) and r_s(parabolic) [Fig. 6(b)] are somewhat different in the spatial diffusion regime although the behavior of the curves $r_s(\beta)$ is similar. The values of r_s(cubic) are smaller since the cubic potential decreases steeper at the descent stage providing less back scattered particles.

B. The influence of the tail of the potential

Figure 6 suggests that the shape of the potential tail can significantly influence the backscattering and thus the decay rate. Therefore, in this section we concentrate on the beyond-barrier shape of the potential and on the location of the absorption point. Results presented in this subsection have

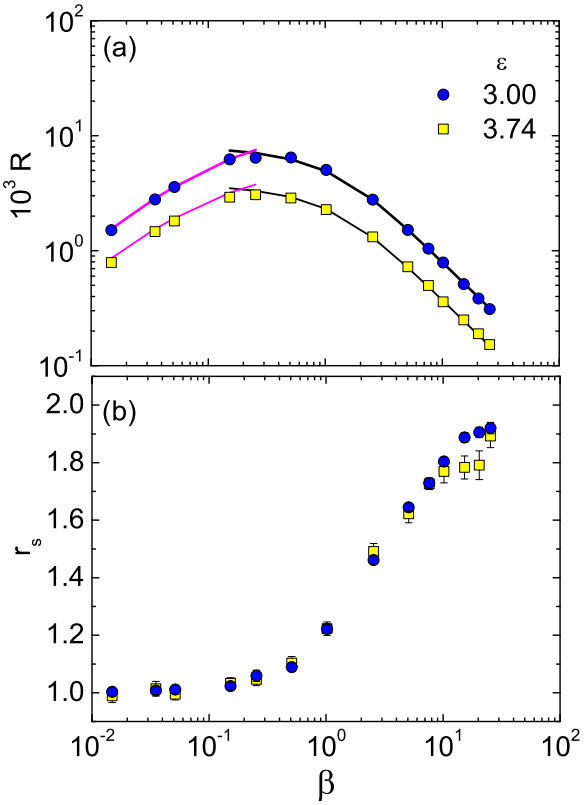

FIG. 5. The same as in Fig. 4 but for two values of ε indicated in panel (a). The lines in that panel correspond to R_{KL} (left side) and R_{KM} (right side). Symbols in panel (a) stand for R_{Das}.

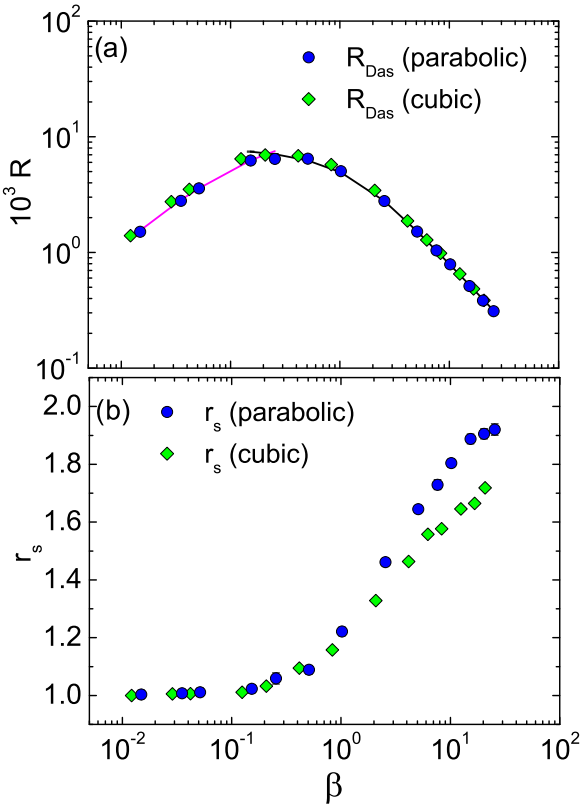

FIG. 6. The same as in Fig. 5 but for two types of the potential energy: parabolic (circles) and cubic (diamonds). The analytical rates R_{KL} (left side) and R_{KM} (right side) are shown by the solid lines in upper panel only for the parabolic potential. $\varepsilon = 3.00$.

been obtained with $\beta = 5.07$. We consider four potentials presented in Fig. 7. The basic one is just the parabolic potential described by Eq. (16).

The other three potentials coincide with the parabolic one at $q < q_j$ and differ beyond q_j. In Fig. 7 $q_j = 1.7$. We have seen in the previous subsection that for the parabolic potential the maximum value of R_D is obtained when the absorptive border q_a simply coincides with the barrier (see Fig. 3). This is equivalent to the potential whose tail drops abruptly at q_a. As a sample of the potential that is close to this but still not abrupt we use the "steep potential" U_S that reads

$$U_S(q) = U_P(q_j) - C_3(q - q_j)^3/3 \text{ at } q > q_j. \tag{19}$$

This potential should result in less backscattering than in the case of the parabolic one. The "linear potential" U_L is defined as

$$U_L(q) = U_P(q_j) + \left(\frac{dU_P}{dq}\right)_{q_j} (q - q_j) \text{ at } q > q_j. \tag{20}$$

It is expected to provide more backscattering than the parabolic one does.

As a limiting case we consider a potential shelf ("flat potential" U_F):

$$U_F(q) = U_P(q_j) \text{ at } q > q_j, \tag{21}$$

which hopefully provides even more backscattering.

Typical behavior of $R_a(t)$ for the four potentials under consideration is shown in Fig. 8. After a transient stage, the decay rate reaches a quasistationary regime although significant fluctuations are present. Duration of the transient stage depends strongly upon the shape of the potential: the steeper the tail, the shorter the transient stage. Thus, care should be taken when choosing the interval for calculating QDR.

There is a discontinuity in the force at q_j for the flat potential. It is possible to make a smooth connection between

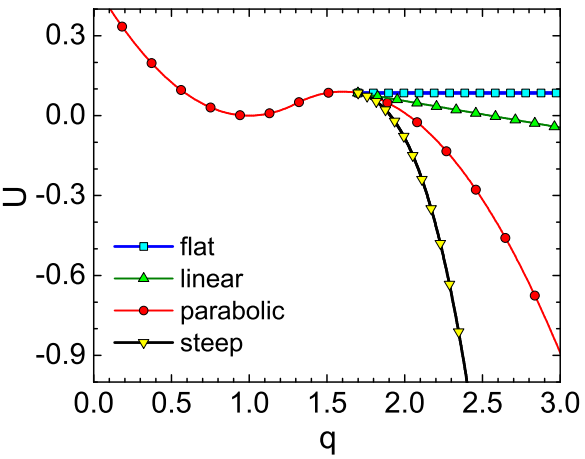

FIG. 7. Four dimenmsionless potentials used in the present work: "flat," "linear," "parabolic," and "steep" [see Eqs. (16), (19)–(21)]. $q_c = 1.0$, $q_b = 1.6$, $q_j = 1.7$.

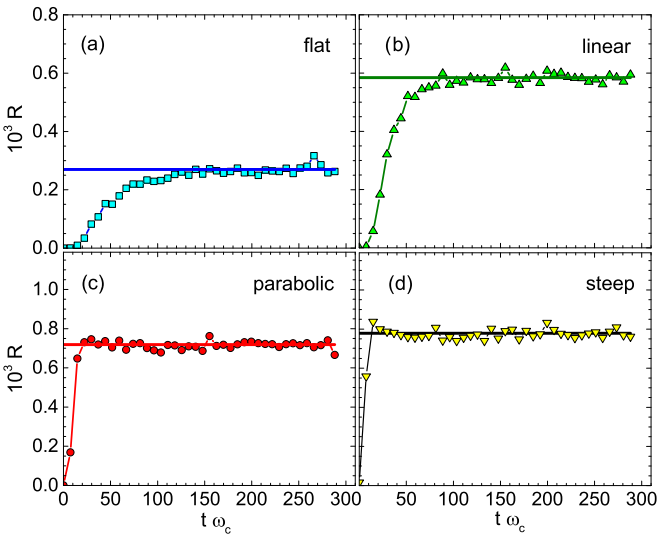

FIG. 8. Typical behavior of the decay rate $R_a(t)$ for the potentials presented in Fig. 7. The horizontal lines indicate the quasistationary dynamical rates. $\varepsilon = 3.75$, $q_j = 1.7$, $q_a = 2.6$, $\beta = 5.07$.

its parabolic and flat parts. We made several calculations with such "smooth-flat" potential and found that the values of QDR for the flat and smooth-flat potentials differ not more than by 1–2%. This is a typical statistical error of our present calculations.

Let us first study what is the role of rescattering at different values of ε and how ZKF measures up against QDR versus ε when the absorptive point is far enough from the barrier ($q_a = 2.6$) and the junction point where our potentials start to differ is rather close to the barrier ($q_j = 1.7$). Results obtained under these conditions are shown in Fig. 9. Since ZKF suggests the exponential dependence of $R_{\rm KM}$ upon ε [see Eqs. (2) and (9)], we present in Fig. 9(a) the dependence $R_D(\varepsilon)$ in the logarithmic scale (scattered symbols). One sees that this dependence is exponential indeed for all the potentials whereas the absolute values are somewhat different indicating the influence of the potential tail. The values of R_D for the flat potential are significantly (by a factor of 3) below the others. To see clearer the difference between R_D and $R_{\rm KM}$ we display in Fig. 9(b) the fractional difference

$$\xi_{\rm MD} = R_{\rm KM}/R_D - 1 \tag{22}$$

with the statistical errors (both in percent) for the parabolic, linear, and steep potentials. The curve corresponding to the flat potential lies significantly higher ($\xi_{\rm MD} \sim 200\%$). Recalling the conditions of applicability of ZKF, one realizes that the best agreement between R_D and $R_{\rm KM}$ for the parabolic potential is to be expected. For the case of the steep potential ZKF underestimates the dynamical rate by some 10% ($\xi_{\rm MD} < 0$), whereas for the linear potential ZKF overestimates the rate by approximately 20% ($\xi_{\rm MD} > 0$).

Let us now come back to Fig. 9(a) and discuss the lines represented there. These lines correspond to the so-called Integral Kramers Formula (IKF). It was discussed in detail in Refs. [17,18,29]. In fact, this formula for the decay rate was implied (but not written explicitly) in the original Kramers paper [1]. As all Kramers rates, this one is based on the "flux

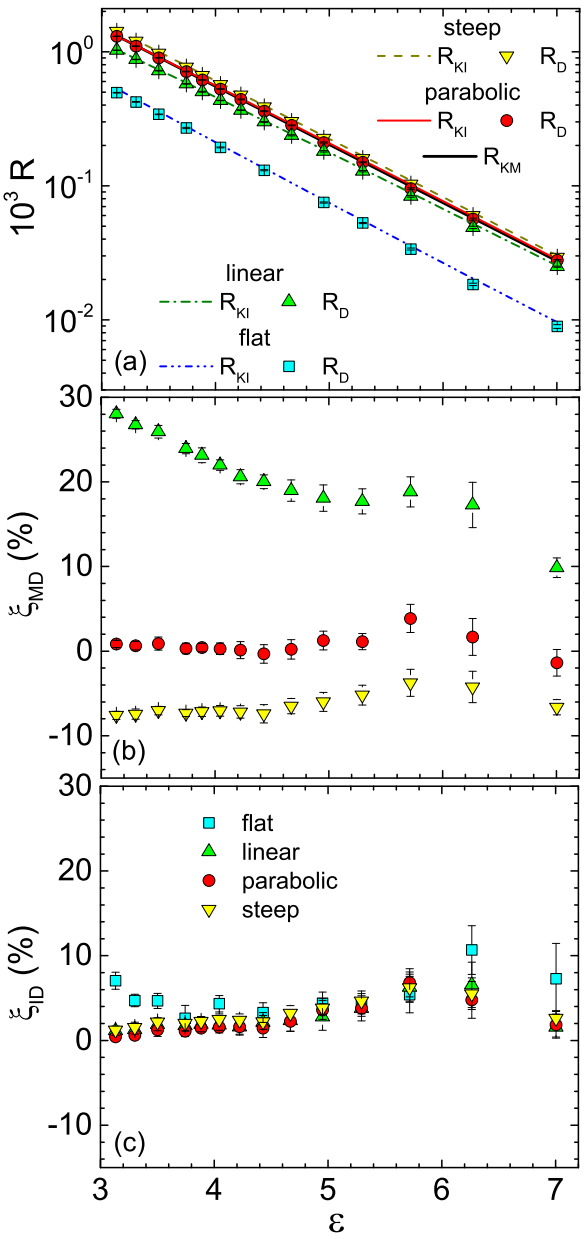

FIG. 9. (a) The quasistationary dynamical rates (symbols) and integral Kramers rates (lines) versus ε for the potentials presented in Fig. 7. Zero-order Kramers rate is shown as well but it is indistinguishable from $R_{\rm KI}$ for the parabolic potential. (b) The fractional difference $\xi_{\rm MD}$ defined by Eq. (22), (c) the fractional difference $\xi_{\rm ID}$ defined by Eq. (25). $q_j = 1.7$, $q_a = 2.6$, $\beta = 5.07$.

over population" method. The dimensionless IKF reads

$$R_{\rm KI} = \frac{U_b}{\beta\varepsilon}\left\{\int_{-\infty}^{q_b}\exp\left[-\frac{\tilde{U}(x)}{\theta}\right]dx \int_{q_c}^{q_a}\exp\left[\frac{\tilde{U}(y)}{\theta}\right]dy\right\}^{-1}. \tag{23}$$

In this equation the integral from $-\infty$ up to q_b represents the population near the quasistationary point, whereas the integral from q_c down to q_a is proportional to 1/(the flux over the potential barrier).

Formally, Eq. (23) is valid in the case of large friction when the motion is overdamped:

$$\frac{\beta^2}{4} \gg 1. \tag{24}$$

In our case $\beta^2/4 = 6.43$, thus inequality Eq. (24) approximately holds. It was shown in Refs. [17,18] that IKF provides a better approximation to QDR in the cases when the potential deviates from the parabolic shape near the barrier and the quasistationary point. In Fig. 9(a) one sees that it is true in our case too. In Fig. 9(c) we quantify the relation between IKF and QDR showing the fractional difference

$$\xi_{\rm ID} = R_{\rm KI}/R_D - 1 \tag{25}$$

in the same scale as in Fig. 9(b). In Fig. 9(c) we see that the values of $\xi_{\rm ID}$ for different potentials are very close to each other. Comparing Figs. 9(b) and 9(c) one notices that the parabolic potential (circles) is the only one for which the values of $\xi_{\rm ID}$ and $\xi_{\rm MD}$ are close to each other. For the linear potential (triangles up) $\xi_{\rm ID}$ lies within 10% whereas $\xi_{\rm MD}$ exceeds 25%. Even for the flat potential (squares), the $\xi_{\rm ID}$ does not exceed 10%, whereas $\xi_{\rm MD}$ estimated from Fig. 9(a) is larger than 200%.

To prove that this is the backscattering which results in the observed mutual relation between the rates [namely, R_D(flat) $< R_D$(linear) $< R_D$(parabolic) $< R_D$(steep)] we register the rescattered particles during our dynamical modeling. There are two features of a particle to be registered as the backscattered one: (i) its coordinate at least once takes a value larger than q_b; (ii) at the end of calculation the coordinate of this particle is smaller than q_b. This simplified algorithm allows us obtaining an estimate for the number of the rescattered particles.

In Fig. 10, we examine the time dependence of this number evaluated numerically, $N_{\rm rs\ num}$, for four potentials under consideration. This quantity divided by the total number of Brownian particles involved in the modeling, $N_{\rm tot}$, is shown by squares, triangles up, circles, and triangles down for the flat, linear, parabolic, and steep potentials, respectively. The statistical errors for all dynamical quantities presented in the figure are within the symbols. We see that, at smaller values of t_D, increasing of the modeling time results in the monotonic growth of $N_{\rm rs\ num}/N_{\rm tot}$ (as well as of $N_{\rm rs\ num}$ itself since $N_{\rm tot}$ is constant). At larger values of t_D, the ratio $N_{\rm rs\ num}/N_{\rm tot}$ saturates. The horizontal line in each panel represents the result of averaging over four last points. Note that the steeper the potential tail, the earlier the saturation.

In addition, we show the ratio $N_{\rm rs\ num}/N_a$ (diamonds) in the same figure where N_a is the number of absorbed particles. One sees that $N_{\rm rs\ num}$ is very significant in comparison with N_a. In contrast to the saturating $N_{\rm rs\ num}$, the number of absorbed particles grows monotonically as the time of modeling increases. Therefore, the ratio $N_{\rm rs\ num}/N_a$ decreases with t_D revealing no saturation.

Results of the rescattered particles registration are presented in Table I for two values of ε. In addition to the ratio $N_{\rm rs\ num}/N_a$, we show here the QDR and the number of rescattered particles evaluated analytically, $N_{\rm rs\ an}$, over N_a. The value of $N_{\rm rs\ an}$ is calculated on the basis of the following consideration.

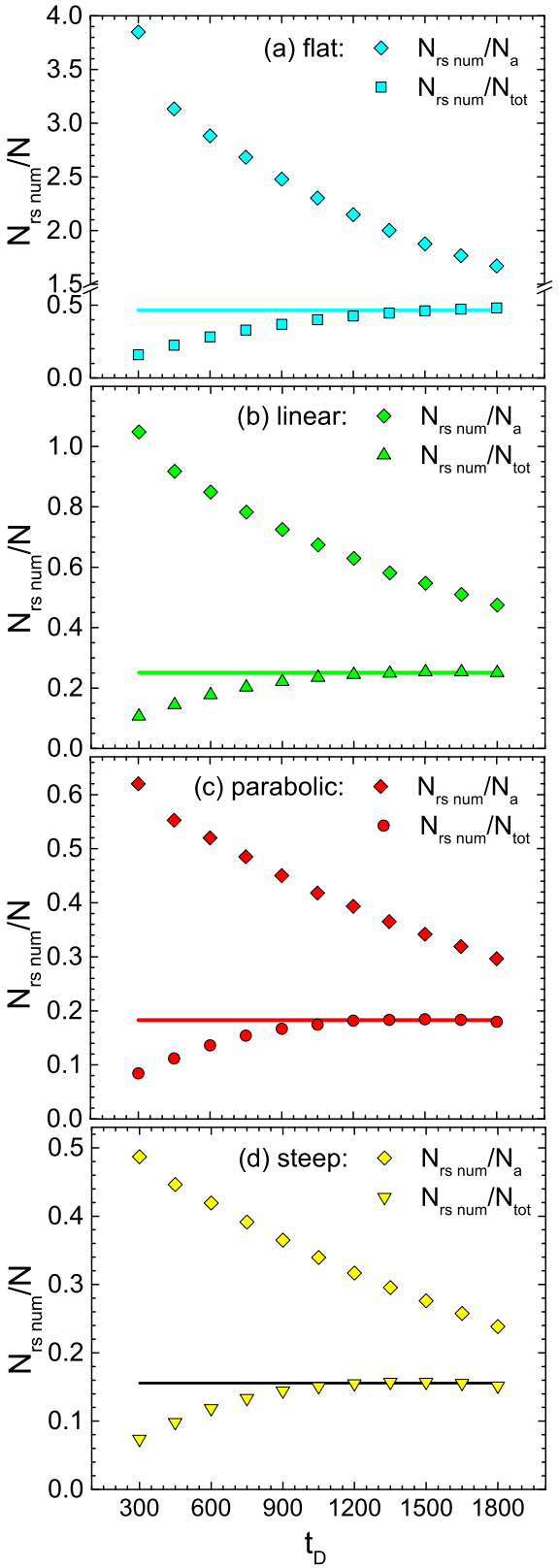

FIG. 10. The number of rescattered particles evaluated numerically over the absorbed particles number (the diamonds) and over the total number of particles involved in the modeling (other symbols) as functions of the modeling time for the potentials presented in Fig. 7. The horizontal lines represent the saturated values of $N_{\rm rs\ num}/N_{\rm tot}$ (see text for details). $\varepsilon = 3.74$.

TABLE I. The quasistationary dynamical rate and the number of rescattered particles evaluated numerically, $N_{\text{rs num}}$, and analytically, $N_{\text{rs an}}$, over the number of absorbed particles, N_a, for four potentials. $\varepsilon = 4.43$ and 3.74; $q_a = 2.6$; $q_j = 1.7$; $N_{\text{tot}} = 5 \times 10^5$; $t_D = 300$ and 600. The adjusting parameter u is explained in the text.

	$\varepsilon = 4.43$; $R_{\text{KM}} = 0.3594\ 10^{-3}$; $u = 1.560$			$\varepsilon = 3.74$; $R_{\text{KM}} = 0.7137\ 10^{-3}$; $u = 1.506$		
	$t_D = 300$			$t_D = 300$		
	R_D, 10^{-3}	$N_{\text{rs num}}/N_a$	$N_{\text{rs an}}/N_a$	R_D, 10^{-3}	$N_{\text{rs num}}/N_a$	$N_{\text{rs an}}/N_a$
Flat	0.1306	3.849	4.276	0.2697	3.688	3.830
Linear	0.2985	0.998	1.043	0.5842	1.048	1.039
Parabolic	0.3587	0.620	—	0.7184	0.611	—
Steep	0.3850	0.504	0.495	0.7786	0.487	0.441
		$t_D = 600$			$t_D = 600$	
Flat	0.1284	3.281	3.925	0.2644	2.637	3.663
Linear	0.3001	0.865	1.011	0.5773	0.774	1.076
Parabolic	0.3553	0.571	0.654	0.7076	0.482	0.648
Steep	0.3833	0.466	0.524	0.7677	0.387	0.504

Neglecting the transient stage, one can estimate the number of non-absorbed particles from the radioactive decay law

$$N_{\text{tot}} - N_a = N_{\text{tot}} \exp(-R_D t_D). \tag{26}$$

In all our calculations $R_D t_D \ll 1$, therefore approximately

$$\frac{N_a}{N_{\text{tot}}} = R_D t_D. \tag{27}$$

It seems reasonable to accept that the number of absorbed particles is just the difference between the number of the particles which have overcome the barrier N_b and the number of rescattered particles N_{rs}:

$$N_a = N_b - N_{\text{rs}}. \tag{28}$$

The number of the particles that have not overcome the barrier should follow the same radioactive decay law but with the rate which is between R_{KM} and $2R_{\text{KM}}$:

$$N_{\text{tot}} - N_b = N_{\text{tot}} \exp(-u R_{\text{KM}} t_D). \tag{29}$$

Here u is still an unknown factor. Since $u R_{\text{KM}} t_D \ll 1$, Eq. (29) results in

$$N_b / N_{\text{tot}} = u R_{\text{KM}} t_D. \tag{30}$$

Combining now Eqs. (27), (28), (30) and excluding N_a and N_b we arrive at

$$N_{\text{rs}} = N_{\text{tot}} t_D (u R_{\text{KM}} - R_D). \tag{31}$$

Now we can estimate N_{rs} analytically ($N_{\text{rs an}}$) if we know u. To find it we first apply Eq. (31) for the parabolic potential using the known numerical value of N_{rs} ($N_{\text{rs num}}$).

In Table I we see that this algorithm provides rather reasonable results. First, u lies between 1 and 2 as we expected. Second, for two rather different values of ε, the values of u are very close. Third, the number of rescattered particles obtained analytically is close to that resulting from numerical modeling. No exact equality between $N_{\text{rs an}}$ and $N_{\text{rs num}}$ is to be expected because in our derivation we neglect the transient stage and multiple rescattering. Indeed, in Fig. 8 we see that the longest transient stage corresponds to the flat potential for which the agreement between $N_{\text{rs an}}$ and $N_{\text{rs num}}$ is the worst. In our opinion, results of Table I and Fig. 10 prove that the inversion of R_D/R_{KM} as the potential goes over from the steep to the flat one is solely due to rescattering.

All the results above are obtained when the absorptive point is far enough from the barrier ($q_a = 2.6$) and the junction point is rather close to the barrier ($q_j = 1.7$). Let us now see how ZKF and IKF measure up against QDR when the absorptive border moves closer and further to the saddle point. The fixed parameters for these calculations are $\varepsilon = 3.17$ and $q_j = 1.70$. The results are shown in Fig. 11. There we see that for the potentials which are "softer" than the parabolic (i.e. decreasing slower after the junction point) ZKF significantly overestimates the true dynamical decay rate. Thus, the mutual layout of R_{KM} and R_D definitely inverses as one switches over from a potential which is steeper than parabolic to the one which is flatter. Moreover, contrary to the cases of the linear, parabolic, and steep potentials, for the flat one R_D does not

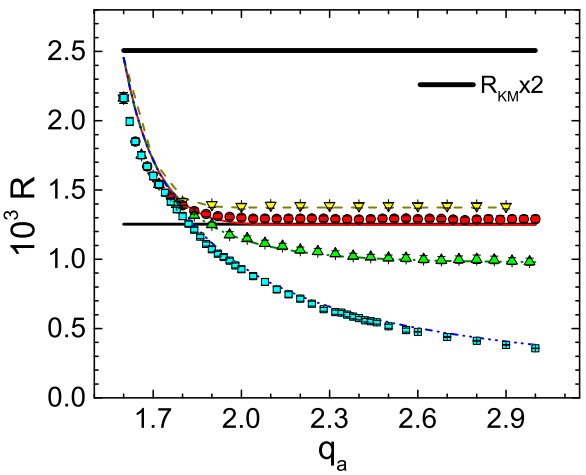

FIG. 11. The quasistationary dynamical rates (symbols) and the rates calculated according to the integral Kramers formula (lines) versus the absorption point coordinate for four potentials presented in Fig. 7. The notations are the same as in Fig. 9(a). The thick solid line in the upper part corresponds to the doubled zero-order Kramers rate. $\varepsilon = 3.17$, $q_j = 1.7$.

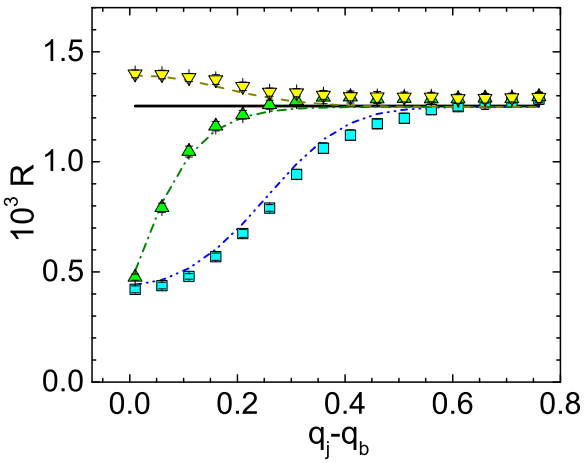

FIG. 12. The same as in Fig. 11 but versus the difference $q_j - q_b$. Results for the parabolic potential are not shown because q_j is not applicable in this case. $\varepsilon = 3.17$, $q_a = 2.6$.

reach any plateau with the increase of q_a. As before, IKF reproduces the numerical QDR nicely at all values of q_a.

Finally, in Fig. 12 we show the evolution of the rates with the increase of the junction point coordinate q_j. As it might be expected, all the rates converge to ZKF as q_j increases.

IV. CONCLUSIONS

We have studied the backscattering of the Brownian particles in their wandering out of the metastable state beyond the barrier. Such backscattering affects the value of the quasistationary decay rate. Usually to model numerically the thermal decay one uses different approaches for different ranges of friction constant. We performed the numerical modeling of this process within the framework of the very same approach, namely by means of the Langevin equations, for the wide range of friction constant covering both the energy and spatial diffusion regimes.

We show how the influence of the descent stage on the quasistationary decay rate gradually disappears as the friction constant decreases. Our present calculations demonstrate that in the energy diffusion regime the rescattering is absent and therefore the descent stage does not influence the decay rate. As the value of friction increases, the descent alters the value of the rate by more than 50%. This effect is stable as we vary the thermal energy and the shape of the potential energy.

For the spatial diffusion regime, the backscattering influences the decay rate significantly. In order to study this influence, four potentials have been considered which coincide near the potential well and the barrier but differ beyond the barrier. The conclusions can be summarized as follows:

(i) the steep potential results in the quasistationary dynamical rate R_D that is larger than the Kramers rate $R_{\rm KM}$ of Eq. (9), whereas for the linear and flat potentials opposite holds (inversion of $R_D/R_{\rm KM}$);

(ii) $R_{\rm KM}$ disagrees with R_D significantly for all but parabolic potential;

(iii) we derived a formula [Eq. (31)], which allows estimating analytically the number of rescattered particles;

(iv) the mutual layout of the values of R_D for different potentials is explained by the rescattering of the particles from beyond the barrier.

ACKNOWLEDGMENTS

M.V.C. acknowledges the warm hospitality of the Department of Physics of Akdeniz University, especially Dr. Haris Dapo. This work was partly supported by the Scientific and Technological Research Council of Turkey (TUBITAK) within the framework of Fellowship Program 2221–for Visiting Scientists and Scientists on Sabbatical Leave. In addition, the authors thank Dr. Anatoliy Ivantsov for the careful reading of the manuscript and useful comments.

APPENDIX: THE LANGEVIN EQUATIONS IN DISCRETE FORM

For the one-dimensional case, the Langevin equations in the discrete form corresponding to the Euler-Maruyama method [30] read

$$p_{n+1} = p_n + \Delta p, \tag{A1}$$

$$q_{n+1} = q_n + \Delta q, \tag{A2}$$

$$\Delta p = -\left(\beta p + \frac{dU}{dq}\right)\tau + b\sqrt{\frac{\beta U_b \tau}{\varepsilon}}, \tag{A3}$$

$$\Delta q = \frac{p_{n+1} + p_n}{2}\tau. \tag{A4}$$

The subscripts refer to two consequent moments of time separated by the time interval $\tilde{\tau} = \tau/\omega_c$, τ is the dimensionless time step of numerical modeling. In the right-hand side of Eq. (A3) all quantities correspond to the time moment $n\tau$. The random numbers b that enter the random forces possess a Gaussian distribution with zero averages and variance equal to 2. In the present calculations the value of τ was typically varied from 0.15 up to 0.60. Each time we checked whether the results of modeling did not depend upon the time step within the statistical errors.

[1] H. A. Kramers, Physica **7**, 284 (1940).
[2] G. Klein, Proc. R. Soc. London A **211**, 431 (1952).
[3] H. C. Brinkman, Physica **22**, 149 (1956).
[4] V. M. Strutinsky, Phys. Lett. B **47**, 121 (1973).
[5] P. Hanggi, P. Talkner, and M. Borkovec, Rev. Mod. Phys. **62**, 251 (1990).
[6] V. I. Melnikov, Phys. Rep. **209**, 1 (1991).
[7] I. I. Gonchar and G. I. Kosenko, Sov. J. Nucl. Phys. **53**, 86 (1991).
[8] G. D. Adeev, A. V. Karpov, P. N. Nadtochy, and D. V. Vanin, Phys. Part. Nucl. **36**, 378 (2005).
[9] Huan-Xiang Zhou, Q. Rev. Biophys. **43**, 219 (2010).
[10] R. E. Lagos and T. P. Simoes, Physica A **390**, 1591 (2011).

[11] P. Talkner and P. Hanggi, *New Trends in Kramers' Reaction Rate Theory* (Springer Science & Business Media, Berlin, 2012).
[12] Z. Jiang, V. N. Smelyanskiy, S. V. Isakov *et al.*, Phys. Rev. A **95**, 012322 (2017).
[13] A. Sharma, R. Wittmann, and J. M. Brader, Phys. Rev. E **95**, 012115 (2017).
[14] C.-C. Chien, S. Kouachi, K. A. Velizhanin, Y. Dubi, and M. Zwolak, Phys. Rev. E **95**, 012137 (2017).
[15] K. Mazurek, P. N. Nadtochy, E. G. Ryabov, and G. D. Adeev, Eur. Phys. J. A **53**, 79 (2017).
[16] M. Buttiker, E. P. Harris, and R. Landauer, Phys. Rev. B **28**, 1268 (1983).
[17] I. I. Gontchar, M. V. Chushnyakova, N. E. Aktaev, A. L. Litnevsky, and E. G. Pavlova, Phys. Rev. C **82**, 064606 (2010).
[18] E. G. Pavlova, N. E. Aktaev, and I. I. Gontchar, Physica A **391**, 6084 (2012).
[19] A. V. Karpov, P. N. Nadtochy, E. G. Ryabov, and G. D. Adeev, J. Phys. G **29**, 2365 (2003).
[20] P. N. Nadtochy, A. Kelić, and K.-H. Schmidt, Phys. Rev. C **75**, 064614 (2007).
[21] E. G. Demina and I. I. Gontchar, Phys. At. Nucl. **78**, 185 (2015).
[22] I. I. Gontchar and M. V. Chushnyakova, Pramana J. Phys. **88**, 90 (2017).
[23] I. I. Gontchar, P. Fröbrich, and N. I. Pischasov, Phys. Rev. C **47**, 2228 (1993).
[24] I. I. Gontchar and P. Fröbrich, Nucl. Phys. A **551**, 495 (1993).
[25] D. Boilley, A. Marchix, B. Jurado, and K.-H. Schmidt, Eur. Phys. J. A **33**, 47 (2007)
[26] A. J. Sierk, Phys. Rev. C **96**, 034603 (2017).
[27] V. L. Litnevsky, V. V. Pashkevich, G. I. Kosenko, and F. A. Ivanyuk, Phys. Rev. C **89**, 034626 (2014).
[28] H. Risken, *The Fokker-Planck Equation* (Springer, Berlin, 1984).
[29] I. I. Gontchar and R. A. Kuzyakin, Phys. Rev. C **84**, 014617 (2011).
[30] P. E. Kloeden and E. Platen, *Numerical Solution of Stochastic Differential Equations* (Springer, Berlin, 1992).